Polar Geometry Waveguides by Finite-Element Methods

P. DALY, MEMBER, IEEE

Abstract—For waveguides whose geometries are described as coordinate surfaces in circular polar coordinates, a finite-element method is used to derive base matrices over a triangular element in the polar geometry. These matrices are used to solve mode problems in circular, sector, double-ridged circular, and spiral waveguides. The discussion is mainly in terms of cutoff frequency, bandwidth, and convergence.

I. Introduction

FINITE-ELEMENT methods [1] have become well established as a means of solving partial differential equations in various branches of engineering. In the electrical sciences, most attention [2], [3] has been directed towards the solution of linear equations for Laplace's equation or eigenvalue equations for the wave equation. In both cases, it is relatively easy in a homogeneous system to formulate a variational expression for some global parameter of the problem, e.g., energy in static problems and wavenumber in wave equation problems. Up to the present, the formulation of the finite-element solution to these problems has been expressed in terms of Cartesian geometry only. In other words, the finite element chosen in two dimensions has been an arbitrary triangle in the xy plane. For problems involving Cartesian boundaries, this approach is clearly more efficient than any other possible choice of element. However, in those cases where the waveguide geometry is not Cartesian, as for example in circular, parabolic, or elliptical waveguides, it is impossible with a Cartesian element to fill the waveguide cross section completely except by a tedious and wasteful limiting process. Isoparametric elements [4] have been used to describe curved boundaries. The function and element boundary behavior are both expressed in terms of the same polynomial expansion. Boundaries which can be described exactly by polynomials can be modeled exactly by the isoparametric element. NonCartesian coordinate surfaces do not fall into this category and require special treatment. Clearly, in those cases where the waveguide geometry can be described in terms of coordinate surfaces where the wave equation is separable, it is of advantage to choose the finite element [5] in that system. In this paper, we discuss solutions of the wave equation in circular polar coordinates for which we define a finite element as a linear triangle in an $r\theta$ coordinate system. The finite-element base matrices for such a choice are then described in some detail, taking account of special difficulties that arise at the origin of such a system. The finite-element matrices are used as building blocks for a particular geometry to construct the matrix equation for the problem by linear superposition of an ensemble of elements.

In view of our experience [6] with Cartesian geometry, we have reason to expect that the rate of convergence on subdividing the mesh will be approximately quadratic for the dominant mode in the absence of any special features such as singular points. From this point of view, and to establish absolute errors, we treat the case of circular and sector waveguides. This initial stage leads us on to the circular double-ridged waveguide [7] which has possibilities (as in rectangular geometry) as a waveguide with reduced dominant mode cutoff and wave impedance, together with increased bandwidth as compared with a waveguide without the ridges. In this respect, the waveguide finds application as a supporting structure for Gunn or IMPATT solid-state devices in the generation of microwave frequencies. The mode structure of the guide is examined and particular attention paid to the dominant H_{11} mode and bandwidth.

The paper is rounded off by a discussion of the spiral waveguide which requires no special treatment in the finite-element method. Some geometries are shown which indicate the range and flexibility of the finite-element method once the base matrices are known and a particular case of spiral waveguide is examined in some detail.

II. Finite Elements in Circular Polars

For a homogeneous uniform waveguide propagating an electromagnetic wave along its axis, it is well known that the longitudinal field ϕ satisfies the variational functional

$$F(\phi) = \iint_S |\nabla_t \phi|^2 \, dS + k^2 \iint_S \phi^2 \, dS \qquad (1)$$

where S is the waveguide cross section and k is the cutoff wavenumber. We use the variational expression as the basis for the development of the finite-element matrices.

In Cartesian geometry, the finite element is a rectilinear triangle in the xy plane, ensuring complete polynomial expressions of the field. In circular polar geometry, the new finite element is again a triangle but now with straight line edges in the $r\theta$ plane; in other words, a triangle in the xy plane whose contours are, in general, circular spirals (see Fig. 1). It is mentioned in passing that the circular arc and radial line are special cases of the spiral. The function ϕ is expressed within the triangle as a linear combination of its point values at the triangle vertices

$$\phi = \Delta^{-1} \sum_{i=1}^{3} \phi_i (a_i r + b_i \theta + c_i) \qquad (2)$$

Manuscript received May 29, 1973; revised November 19, 1973.
The author is with the Department of Electrical and Electronic Engineering, University of Leeds, Leeds, England.

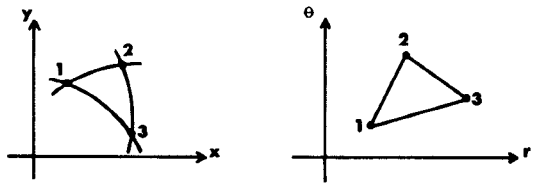

Fig. 1. The circular polar finite element in the xy and $r\theta$ plane.

where

$$a_i = \theta_j - \theta_k \qquad b_i = r_k - r_j$$
$$c_i = r_j\theta_k - r_k\theta_j \tag{3}$$

using cyclic notation mod 3 and

$$\Delta = \sum_{i=1}^{3} \theta_i(r_j - r_k) = \sum_{i=1}^{3} r_i(\theta_k - \theta_j). \tag{4}$$

Clearly

$$\sum_{i=1}^{3} a_i = \sum_{i=1}^{3} b_i = 0 \qquad \sum_{i=1}^{3} c_i = \Delta. \tag{5}$$

It is convenient when working out the finite-element matrices to use a coordinate system $W_i = 1,2,3$, where we define W_i as

$$W_i = a_i r + b_i\theta + c_i. \tag{6}$$

Equation (2) reduces to the simple form

$$\phi = \Delta^{-1} \sum_{i=1}^{3} \phi_i W_i \tag{7}$$

with

$$r = \sum_{i=1}^{3} r_i W_i \qquad \theta = \sum_{i=1}^{3} \theta_i W_i \tag{8}$$

and

$$\sum_{i=1}^{3} W_i = 1 \tag{9}$$

indicating the interdependence of the new coordinates.

We are now in a position to substitute for ϕ from (7) into (1) and differentiate with respect to ϕ_i, $i = 1,2,3$. Carrying out the resulting integrations over a single element E, we arrive at the basic finite-element matrix equation holding for a single triangle in the cross section

$$S_{mn}\phi_n = k^2 T_{mn}\phi_n \tag{10}$$

where ϕ_n is the column vector $[\phi_1,\phi_2,\phi_3]$ and S_{mn} and T_{mn} are 3×3 symmetric positive-definite finite-element matrices for the polar triangle.

They are easily shown [5] to be given by

$$\Delta^2 S_{mn} = a_m a_n \iint_E r\, dr d\theta + b_m b_n \iint_E r^{-1}\, dr d\theta \tag{11}$$

and we find on evaluation of the integrals that

$$\Delta S_{mn} = a_m a_n F + b_m b_n G \tag{12}$$

where

$$F = \frac{1}{6} \sum_{i=1}^{3} r_i \tag{13}$$

$$G = -\sum_{i=1}^{3} r_i(r_i - r_j)^{-1}(r_k - r_i)^{-1} \ln r_i \tag{14}$$

using cyclic notation and

$$T_{mn} = \frac{\Delta}{60}(3r_i + r_j + r_k), \qquad m = n = i$$
$$= \frac{\Delta}{120}(2r_i + 2r_j + r_k), \qquad m = i, \quad n = j, \quad m \neq n. \tag{15}$$

The quantity G becomes indeterminate under certain circumstances which are dealt with as follows.

1) If one radial coordinate is zero, say r_i, then

$$G = (r_j - r_k)^{-1} \ln r_j/r_k. \tag{16}$$

2) As in 1), but $r_j = r_k$, then

$$G = 1/r_j. \tag{17}$$

3) If two radial coordinates are equal and nonzero, say $r_i = r_k \neq 0$, then

$$G = (r_k - r_j)^{-2}[r_k \ln (r_k/r_j) - (r_k - r_j)]. \tag{18}$$

4) As in 3), but $r_i = r_k = 0$.

Here we have the intriguing prospect which does not arise in Cartesian geometry of an element with only two separate points in it, one of them at the origin of the xy plane. This is because if two points have the same value of radial coordinates, namely zero, the value of ϕ at the two points must be the same since the distance between the points is zero. In Cartesian geometry, the area of such an element would be zero, but not so in polar geometry. In order to derive the matrices (2×2) for this special case, we assume that, say, $r_i = r_k = 0$. Then, since $\phi_i = \phi_k$, $\theta_i \neq \theta_k$, we use the expression

$$\phi = \Delta^{-1}[\phi_i(1 - W_j) + \phi_j W_j] \tag{19}$$

in the variational formula (1) as previously. Carrying out the necessary operations we find that

$$\Delta S_{mn} = (\theta_i - \theta_k)^2(-1)^{m+n}F, \qquad m,n = 1,2 \tag{20}$$

$$T_{mn} = \frac{\Delta}{20} r_j, \qquad m = n$$
$$= \frac{\Delta}{30} r_j, \qquad m \neq n \tag{21}$$
$$\Delta = r_j(\theta_k - \theta_i).$$

The result for T_{mn} can easily be obtained from (15) by setting $r_i = r_k = 0$ and reducing the matrix. For the purposes of computation, it is more efficient to treat the last special case as if the triangle had three separate labeled

points and to program the matrix entries appropriately. In any case, possession of the matrices S and T allows us to solve any waveguide problem where the boundaries form parts of spiral contours. We are also guaranteed that all eigenvalues of the matrix equation will be upper bounds to the exact cutoff wavenumbers of the problem. It is usually extremely difficult when using finite elements in eigenvalue problems to estimate the absolute error in the computed eigenvalues. The rate of convergence of the solution with decreasing element size is something which is more easily found. In the case of a cross section with no singular points, i.e., points at which first derivatives of the field become infinite, the error is reduced quadratically with mesh size. For modes other than the dominant or for geometries including a singular point, e.g., the double-ridged waveguide which occurs later, the rate of convergence is lower and, in the worse case, decreases linearly with mesh size. In this paper, we attempt to establish the rate of convergence and absolute error of the eigenvalue on an ad hoc basis and to use these results together with Aitken's δ^2 process [8] to extrapolate.

III. Applications

A. Circular and Sector Waveguide

The most straightforward application of the finite-element method in polar geometry is clearly the circular waveguide which we examine to test our method and establish rates of convergence and absolute error bounds. We examine one quadrant of a circular waveguide with boundary conditions appropriate to H_{nm} modes with n odd. This waveguide is shown in the xy and $r\theta$ planes, respectively, in Fig. 2, together with the splitting up of the region into finite elements. The letters N and D on the boundary denote Neumann ($\partial\phi/\partial n = 0$) and Dirichlet ($\phi = 0$) conditions, respectively. Note that in this cross section there are two elements touching the origin having only two points per element. In Fig. 2(b) the single point at the origin is represented by the axis $r = 0$. By linearly superposing the finite-element matrices for each element in turn, we build up a single matrix equation whose eigenvalues are k^2 and whose eigenvector is a list of the function values at nodal points.

Beginning with the simple mesh shown in Fig. 2, we subdivide the cross section uniformly producing a quadratic increase in the dimension N of the overall matrix

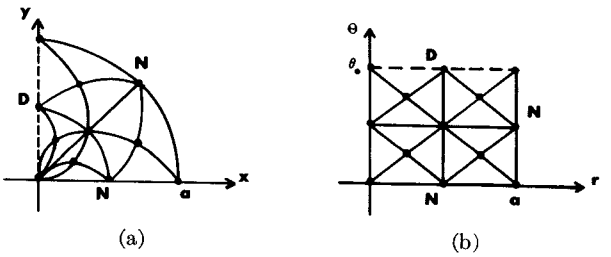

Fig. 2. Quadrant of a circular waveguide showing the division of the cross section into finite elements. Neumann (N) and Dirichlet (D) boundary conditions are shown.

TABLE I
Cutoff Wavenumber for Odd H Modes in Circular Waveguide

N	H_{11}	H_{31}	H_{12}	H_{51}	H_{32}	H_{13}
8	1.938	4.970	6.214	10.907	9.735	13.883
32	1.869	4.388	5.601	7.173	8.607	9.552
128	1.849	4.247	5.405	6.605	8.154	8.819
extrapolated	1.843	4.213	5.342	6.519	7.972	8.695
quadratic	1.842	4.200	5.340	6.416	8.002	8.575
exact[9]	1.841	4.201	5.331	6.416	8.015	8.536

equation. Results are presented in Table I for the cutoff wavenumber ka against matrix order N for the first six odd H modes in the circular waveguide. These are compared with exact values [9] obtained from the zeros of the appropriate Bessel function. Extrapolated values are also given based on Aitken's δ^2 process involving three successive estimates to a quantity. Lastly, a row entitled "quadratic" is given which computes an approximation based on two successive estimates assuming quadratic decrease in the error. The results headed "quadratic" are based on the last two estimates ($n = 32$ and 128) and confirm the assumption on which they are based. The extrapolated results do not compare favorably with the "quadratic" estimate, at least for the higher modes, since they involve the least accurate results ($n = 8$) where the error behavior is erratic. The unsettled error behavior arises because there are too few points in the cross section to adequately describe the field dependence. In the terminology of the communications engineer, the Nyquist or sampling rate of the field is below threshold. At any rate, the error behavior for the dominant mode is approximately quadratic and becomes so for higher order modes when sufficient points exist to describe their fluctuations well. In absolute terms, we find, as expected, the error least for the dominant mode and increasing with the complexity of the mode. For the largest matrix tried, the error for the dominant mode is less than 0.5 percent and increases to ~3 percent in the worst case.

Owing to the uniformity of the waveguide along the θ axis with homogeneous boundary conditions at the ends, the computed eigenvector shows the exact [6] behavior along the θ axis, i.e., points on the same radial line are related by the appropriate cosine or sine behavior. This behavior provides a useful check to the programmer.

If the angle θ_0 of Fig. 2(b) is varied between 0 and 360°, we produce the class of waveguides known as sector [10] waveguides, since their walls form the sides of a circular sector. The cutoff wavenumber of the dominant mode is compared with the results of a finite-element analysis as a function of section angle in Table II. This example is particularly apt in that as θ_0 is varied, the point at the origin describes all the possible types of singularity we are likely to meet in waveguides. No extra programming is required for these cases, since a single data card informs the computer of the value of θ_0. From the results of Table

TABLE II
CUTOFF WAVENUMBER OF THE DOMINANT MODE IN SECTOR WAVEGUIDE ka

n \ θ_0	30	60	90	135	180
8	4.498	2.610	1.938	1.504	1.304
32	4.263^{235}	2.494^{116}	1.869^{69}	1.440^{64}	1.232^{72}
128	4.216^{47}	2.468^{26}	1.849^{20}	1.416^{24}	1.198^{34}
exact	4.201	2.461	1.841	1.401	1.166

II we can make some comments about the rate of convergence in the presence of a singular point. By differencing successive approximations, we see that the error decreases most slowly (almost linearly) for the 360° corner ($\theta_0 = 360°$) and most rapidly (better than quadratic) where there is no singular point and θ_0 is smallest ($\theta_0 = 30°$). The in-between case studied previously ($\theta_0 = 90°$) shows the standard quadratic error behavior. The linear behavior for the 360° corner arises because the first derivative of the potential is infinite and therefore discontinuous.

The special cases of circular and sector waveguides indicate that we can hope for, at best, quadratic convergence of the eigenvalue to the exact value with an absolute error in the extrapolated eigenvalue not exceeding 1 percent for matrix orders over 100.

B. Double-Ridged Circular Waveguides

We turn now to an important class of polar geometry waveguide whose solution is new and which could have important application as a supporting structure in the generation of microwave frequencies by means of the Gunn diode, IMPATT, and other solid-state devices. This waveguide is the double-ridged circular waveguide [7] whose cross section in the first quadrant is shown in Fig. 3, for the special case $\bar{r} = r_0/a = 1/2$, $\theta_0 = \pi/4$. The boundary conditions are those for H modes having odd symmetry about the y axis and even symmetry about the x axis. The lowest order of these modes is clearly the dominant mode which we call the H_{11} since it is the perturbed version of the H_{11} mode in the circular waveguide. A second H_{11} mode exists whose symmetry about the x and y axes is reversed. In fact, every mode of the circular guide has its two-fold degeneracy split by the introduction of the ridge into the waveguide. In Fig. 3, the cross section is shown split up into 12 elements and 7 labeled points taking account of the zero field condition on the y axis. This is the simplest division chosen and forms the starting point for more sophisticated subdivisions. We examine the cutoff wavenumbers ka of the first three H modes of the waveguide in Fig. 3 on the basis of the division shown and two further subdivisions each time doubling the number of labeled points, d along the x or r axis, and approximately squaring the matrix order N. The results are presented in Table III together with extrapolated values obtained by means of Aitken's δ^2 process. The rate of convergence for

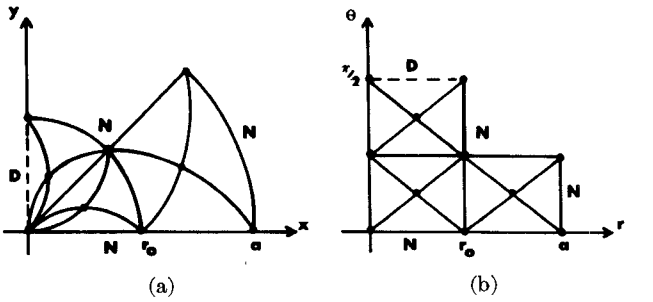

(a) (b)

Fig. 3. Quadrant of a double-ridged circular waveguide showing the division of the cross section into finite elements.

TABLE III
CUTOFF WAVENUMBER FOR ODD H MODES IN DOUBLE-RIDGED WAVEGUIDE

d	N	H_{11}	H_{31}	H_{12}
2	7	1.625	6.134	5.901
4	26	1.508	5.739	5.340
8	100	1.469	5.429	5.153
extrapolated		1.456	5.175	5.103

$\bar{r} = 1/2$; $\theta_0 = \pi/4$.

the H_{11} mode is approximately quadratic and is the best rate we might expect, considering the presence of the singular point of the ridge. Taking account of the quadratic convergence and the earlier results on the sector waveguide with a $3\pi/2$ corner, the absolute error in the dominant mode eigenvalue can be expected not to exceed 1 percent. This view is born out by the extrapolated value. Rates of convergence for the H_{31} and H_{12} modes are rather poorer than for the dominant modes owing to the fact that their eigenvectors vary much more rapidly over the cross section. It is safe to assume that the wavenumbers for the smallest subdivision ($d = 8$) are correct to within a few percent. Acting on these assumptions concerning error rate, we have computed the dominant H_{11} mode cutoff ka for a range of values of ridge dimensions using the mesh subdivision which gives $d = 8$. These results are shown in Fig. 4 with k/k_c plotted along the vertical axis (k_c is the cutoff wavenumber for circular waveguide of radius a). Clearly, a reduction in the cutoff frequency of the dominant mode is possible for a large variety of ridge dimensions. Since the wave impedance is defined using standard notation as

$$Z_w = \frac{\omega\mu}{\beta} = \left(\frac{\mu}{\epsilon}\right)^{1/2}\left(\frac{\omega a}{c}\right)\left[\left(\frac{\omega a}{c}\right)^2 - (ka)^2\right]^{-(1/2)}$$

it is also reduced at a given frequency below its value in the circular waveguide of the same outer radius. The double-ridged waveguide thus has possible advantages over conventional circular waveguides in that the wave impedance is reduced and that the waveguide dimensions are reduced for a fixed frequency of propagation. It remains to be seen how the waveguide bandwidth varies as a function of the ridge parameters.

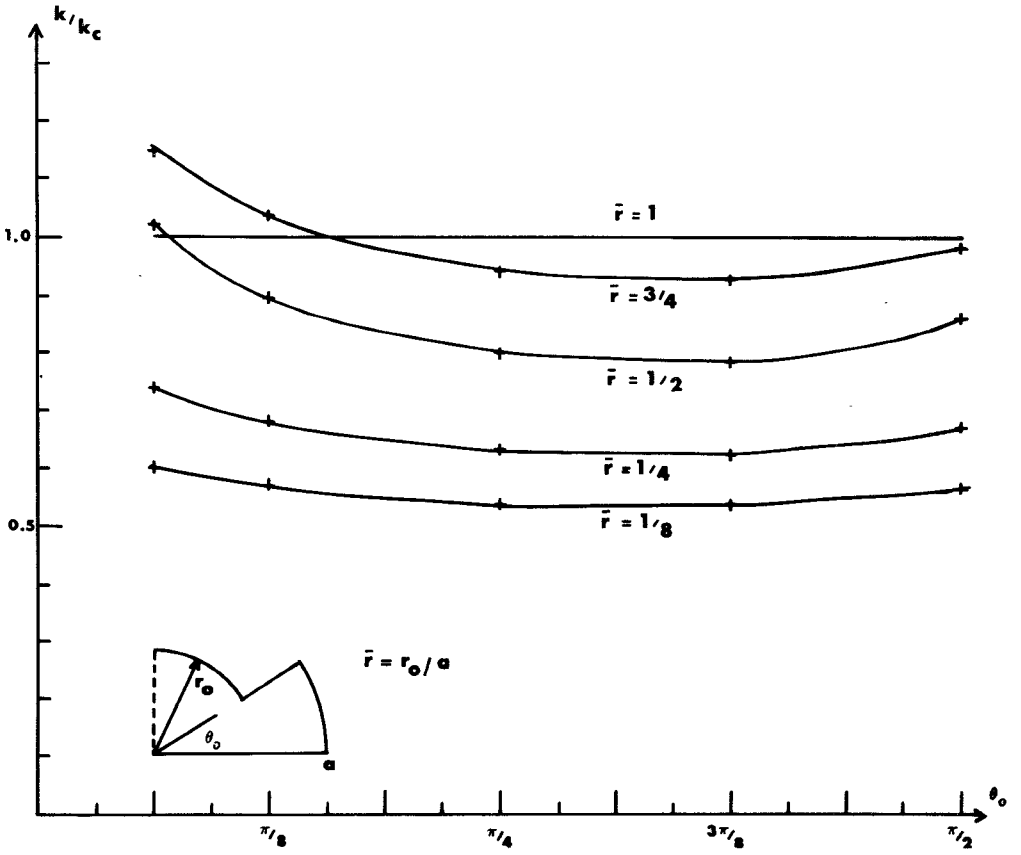

Fig. 4. Cutoff wavenumber of double-ridged circular waveguide as a function of ridge parameters.

TABLE IV
CUTOFF WAVENUMBER IN DOUBLE-RIDGED WAVEGUIDES FOR BOTH E AND H MODES

N	mode	y-axis	x-axis	ka	ka ($\bar{r}$ = 1)
26	H_{11}	D	N	1.508	1.841
24	H_{11}	N	D	3.102	1.841
29	H_{01}	N	N	3.132	3.832
22	H_{21}	D	D	3.252	3.054
18	E_{11}	N	D	7.898	3.832
20	E_{11}	D	N	5.004	3.832
22	E_{01}	N	N	4.103	2.405
17	E_{21}	D	D	8.109	5.136

$\bar{r} = 1/2; \theta_0 = \pi/4$.

We begin by taking the waveguide of Fig. 3 and computing the cutoff wavenumbers of the lowest modes for both E and H modes, allowing all possible symmetries on the axes. A fairly crude mesh is used ($d = 4$) since it is intended only to gain a qualitative picture of the effect of the ridge on the cutoff frequencies. These solutions are presented in Table IV, together with those for the corresponding circular waveguide. It is interesting to note that the H_{11} mode with odd symmetry about the x axis has its cutoff frequency sharply increased as do the E_{01} and E_{11} modes. In order to define bandwidth we must consider the means of excitation of the dominant mode. Assuming this to be such that only those modes having the same symmetries as the dominant mode can exist, the bandwidth is defined as the difference between the lowest and next-to-lowest cutoff frequencies. This is shown in units of ka for the dominant mode of circular waveguides as a function of the ridge dimensions in Fig. 5 with the bandwidth of circular waveguide shown for comparison. If θ_0 is taken to be around 45°, increases in bandwidth can be combined

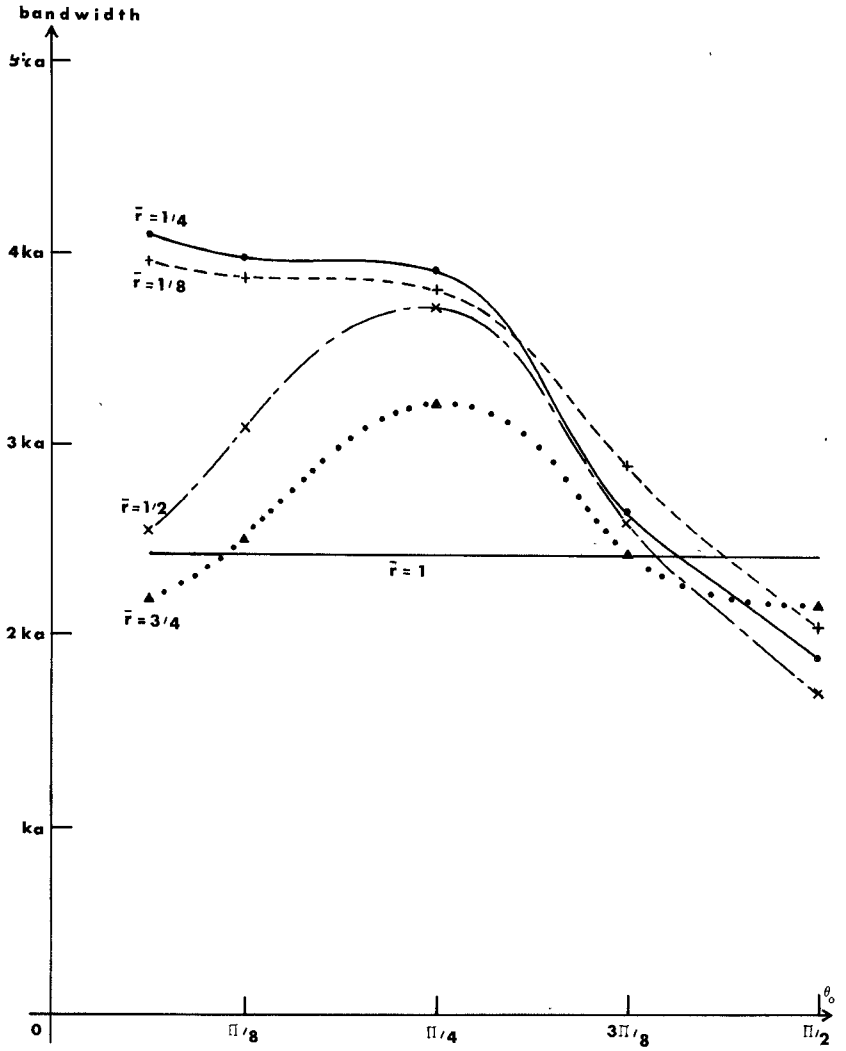

Fig. 5. Bandwidth of double-ridged circular waveguide in units of ka of circular waveguide.

with a low figure of cutoff frequency. It is curious to note that the bandwidth does not increase indefinitely but for values of $\bar{r}$ less than $\frac{1}{4}$ levels off. This occurs because the ridge fills such a large portion of the cross section that it affects equally the dominant and next higher order mode.

We complete discussion of the double-ridged waveguide by showing the field behavior of the first three odd H modes. These are shown in Fig. 6 as lines of constant longitudinal magnetic field or transverse electric field normalized to a maximum value of ten. These results are given directly by the computer as the eigenvectors of the problem and can be produced by graph plotter. The remaining field components if required are found by a process of numerical differentiation.

C. Spiral Waveguides

We complete the treatment of general cylindrical polar geometry waveguides with a discussion of spiral waveguides, i.e., any waveguide whose boundaries form segments of circular spirals. The number of possibilities is naturally infinite but we display several which are of some interest in Fig. 7. Each of these cross sections consists of straight-line segments in the $r\theta$ plane and therefore is amenable to a direct analysis by the finite-element method. We choose to examine the waveguide shown in Fig. 8 with a simple choice of finite elements. Note that the points on the θ axis in Fig. 8(b) all have the same function value. In looking for the dominant mode as a function of θ_0 we find those of waveguide "pisces" of Fig. 7 when $\theta_0 = \pi/2$ and those of the waveguide "heart" of Fig. 7 when $\theta_0 = \pi$. These results are shown in Table V as a function of matrix dimensions for modes possessing an electric wall along the x axis. We note that for the dominant mode the rate of convergence is almost quadratic for both values of θ_0. This confirms our view derived from earlier results. In comparing the results with those for a circular waveguide of radius a, we observe the same mode structure except for the absence of the low-loss H_{01} mode in a spiral waveguide which is owing to the presence of the sharp corners in the cross section.

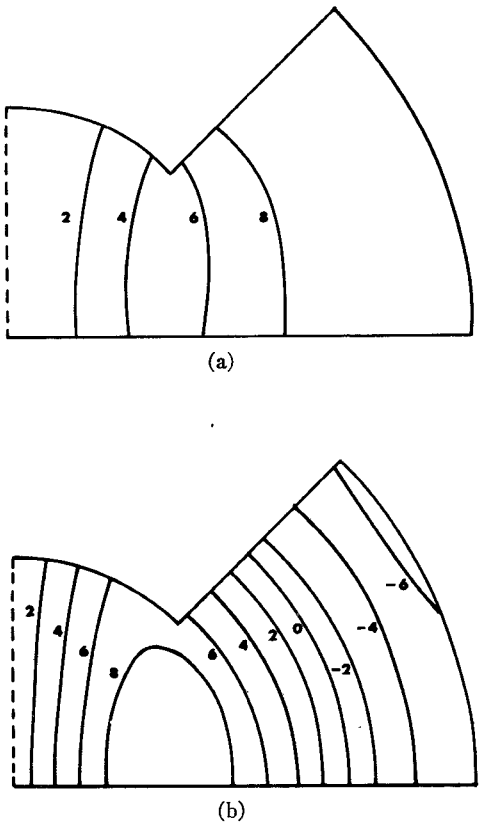

Fig. 6. Field dependence of the first three H modes in a double-ridged circular waveguide having even and odd symmetry about the y and x axes, respectively. (a) H_{11}. (b) H_{12}. (c) H_{31}.

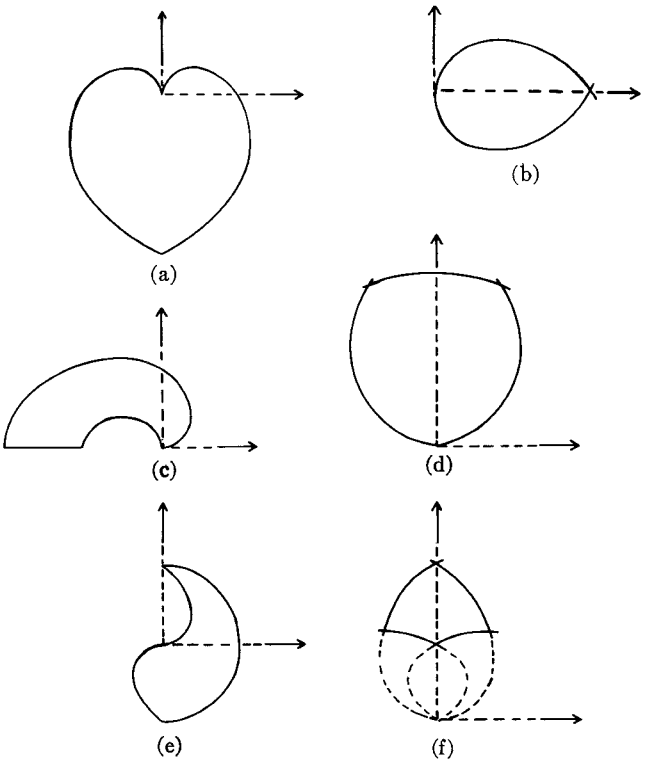

Fig. 7. Some possible waveguide shapes with spiral contours. (a) Heart. (b) Pisces. (c) Snail. (d) Shield. (e) Ying-yang. (f) Norman.

TABLE V
CUTOFF WAVENUMBER FOR A SPIRAL WAVEGUIDE ka

		$\theta_0 = \pi/2$			$\theta_0 = \pi$		
d	N	H_{11}	H_{21}	H_{31}	H_{11}	H_{21}	H_{31}
2	9	2.162	4.334	5.820	1.811	3.615	4.383
4	33	2.000	3.826	5.238	1.650	3.155	3.466
8	129	1.963	3.520	4.947	1.605	2.843	3.269
extrapolated		1.954	3.336	4.802	1.593	2.633	3.227

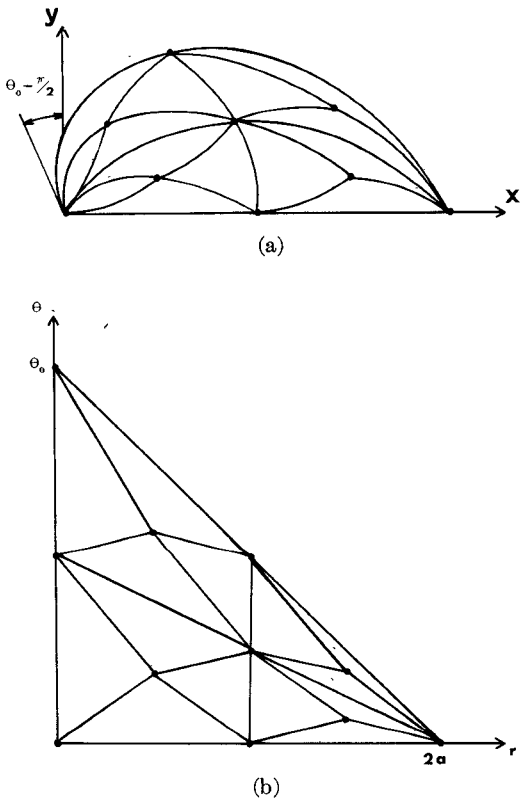

Fig. 8. A spiral waveguide showing mesh subdivision in the xy and $r\theta$ planes.

IV. Conclusions

The finite-element method for cylindrical polar geometries has been developed and applied to circular and sector waveguides to establish rates of convergence and absolute errors in cross sections with and without singular points. The mode structure of the double-ridged waveguide has been established for various symmetries and it is concluded that the waveguide has the advantages over the circular waveguide of 1) reduced cutoff frequency and wave impedance and 2) increased bandwidth. The most general type of waveguide in polar geometry directly solvable by this method has spiral boundaries. Examples of these have been given and particular cases studied. It is clear that other geometries not described here but nevertheless interesting might also be solved by the method. There is, for example, a whole class of problems involving coaxial structures where the solution of Laplace's or Helmholtz's equation might be required. This generalization of the usual finite-element method allows boundaries linear in an $r\theta$ coordinate system to be treated exactly and effectively removes from consideration the need to treat [11] truncation error at curved boundaries.

References

[1] O. C. Zienkiewicz, *The Finite Element Method in Engineering Science*. London, England: McGraw-Hill, 1971.

[2] P. Silvester, "High-order polynomial triangular finite-element for potential problems," *Int. J. Eng. Sci.*, vol. 7, pp. 849–861, 1969.

[3] A. Wexler, "Computation of electromagnetic fields," *IEEE Trans. Microwave Theory Tech. (Special Issue on Computer-Oriented Microwave Practices)*, vol. MTT-17, pp. 416–439, Aug. 1969.

[4] J. Ergatoudis, B. M. Irons, and O. C. Zienkiewicz, "Curved isoparametric quadrilateral elements in finite element analysis," *Int. J. Solid Structures*, vol. 4, pp. 31–42, 1968.

[5] P. Daly, "Finite-elements for field problems in cylindrical coordinates," *Int. J. Num. Meth. Eng.*, vol. 6, no. 2, pp. 169–178, 1973.

[6] P. Daly and J. D. Helps, "Exact finite-element solutions to Helmholtz's equation," *Int. J. Num. Meth. Eng.*, vol. 6, no. 4, pp. 529–542, 1973.

[7] A. M. A. El-Sherbiny, "Cutoff wavelengths of ridged, circular, and elliptic guides," *IEEE Trans. Microwave Theory Tech.*, vol. MTT-21, pp. 7–12, Jan. 1973.

[8] M. Abramowitz and I. A. Stegun, *Handbook of Mathematical Functions*. New York: Dover, p. 18.

[9] ——, *Handbook of Mathematical Functions*. New York: Dover, p. 411.

[10] R. H. T. Bates and F. L. Ng, "Point matching computation of transverse resonances," *Int. J. Num. Meth. Eng.*, vol. 6, no. 2, pp. 155–168.

[11] D. J. Richards and A. Wexler, "Finite-element solutions within curved boundaries," *IEEE Trans. Microwave Theory Tech.*, vol. MTT-20, pp. 650–657, Oct. 1972.

The Solution of Inhomogeneous Waveguide Problems Using a Transmission-Line Matrix

PETER B. JOHNS

***Abstract*—A method of applying the transmission-line matrix method to inhomogeneous waveguide structures is described. The technique uses open-circuit stubs of variable characteristic impedance at each node in the matrix, thereby providing an analog for a dielectric. LSE and LSM modes in rectangular waveguides, and problems involving a step of dielectric are solved. Results are given in terms of the cutoff frequency and field pattern for continuous waveguides, and the waveguide input impedance for scattering problems.**

Introduction

THE transmission-line matrix method has been used to solve scattering problems in waveguides [1] and also to obtain the cutoff frequencies for waveguides of arbitrary cross section [2]. In both cases, the waveguides were assumed to be filled with a homogeneous medium. In applying the principles of the transmission-line matrix method to random walk analysis [3], results were obtained for a one-dimensional inhomogeneously filled waveguide. However, there is a large class of inhomogeneous waveguide problems that require solution in two space dimensions and an application technique for the transmission-line matrix method in such cases is introduced in this paper.

Manuscript received June 1, 1973; revised September 14, 1973.
The author is with the Department of Electrical and Electronic Engineering, University of Nottingham, Nottingham, England.

Matrix Configuration and Properties

In [1] and [2], propagation in a two-dimensional medium is represented by the voltages and currents on a Cartesian mesh of TEM transmission lines. Analysis of the mesh is accomplished by considering an impulsive excitation and following the progress of impulses as they propagate throughout the matrix. The mesh is represented at each node by a submatrix of four numbers describing